Supplementary Material

Photoelectrochemical water splitting at low applied potential using NiOOH coated codoped (Sn, Zr) α-Fe_2O_3 photoanode

Andebet Gedamu Tamirat[a], Wei-Nien Su*[b], Amare Aregahegn Dubale[a], Hung-Ming Chen[a], and Bing-Joe Hwang*[ac]

[a]NanoElectrochemistry Laboratory, Department of Chemical Engineering, National Taiwan University of Science and Technology, Taipei, 106, Taiwan. E-mail: bjh@mail.ntust.edu.tw; Fax: +886-2-27376644

[b]NanoElectrochemistry Laboratory, Graduate Institute of Applied Science and Technology, National Taiwan University of Science and Technology, Taipei 106, Taiwan

[c]National Synchrotron Radiation Research Center, Hsinchu, 30076, Taiwan

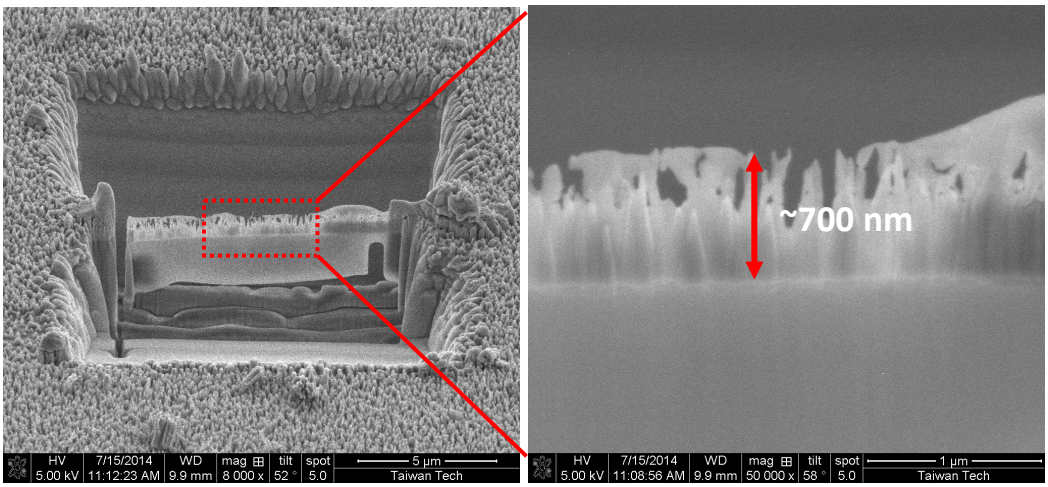

Figure S1. SEM image of the codoped (Sn, Zr) Fe_2O_3 nanorod arrays modified with NiOOH with a FIB prepared cross-section. The particles on the surface of the film come from the Pt deposited prior to the SEM measurement to increase surface electrical conductivity and to prevent charge buildup.

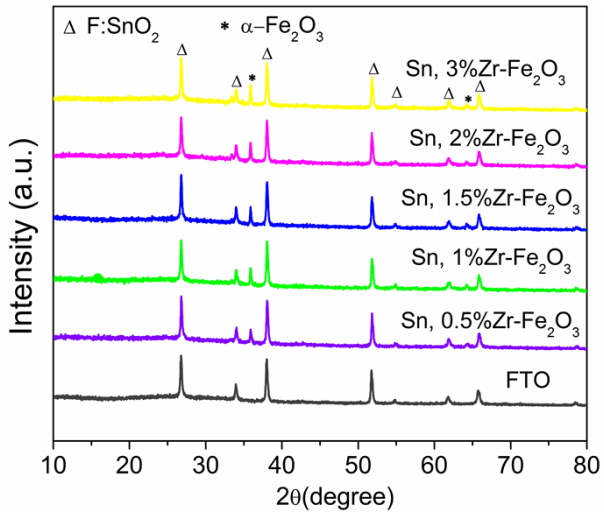

Figure S2. XRD pattern of codoped (Sn, Zr) Fe_2O_3 with different atomic percentage of Zr.

The approximate band gap of all the samples is determined from Tauc plots (Figure S3). Because hematite is a type of indirect semiconductor, the curves of $(\alpha hv)^{1/2}$ versus hv were plotted according to the following equation[1, 2]:

$$\alpha hv = A(hv - E_g)^2 \quad (1)$$

where α is the absorption coefficient, A is a proportional constant, h is Planck's constant, v is the photon frequency, and E_g is the optical band gap energy. Using a linear fit for the straight interval in the region of largest exponential growth; the intercept to the energy axis corresponds to the optical band gap.

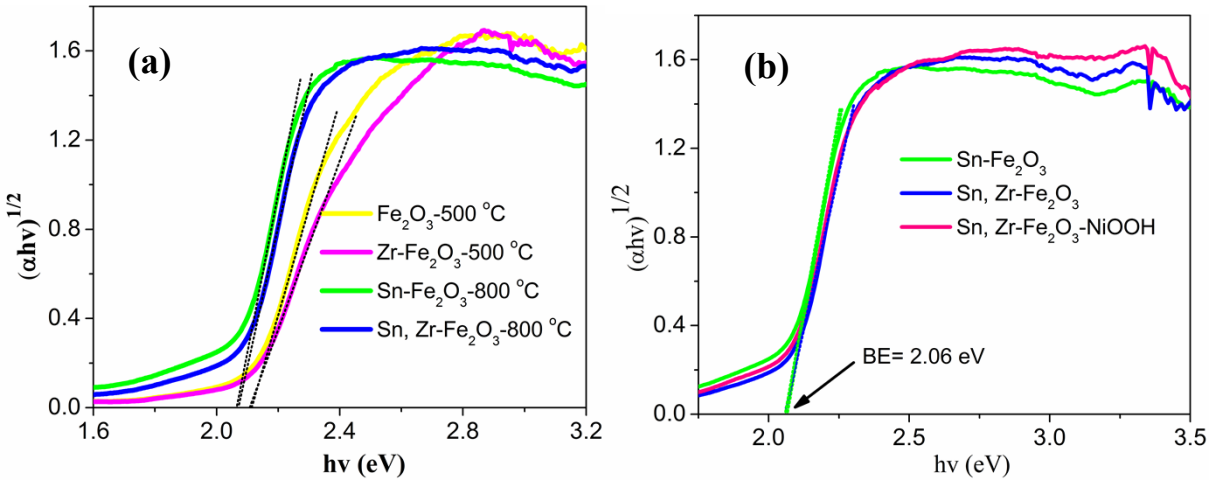

Figure S3. Plot of Kubelka-Munk-transformed diffuse reflectance spectra versus energy of the light transformed.

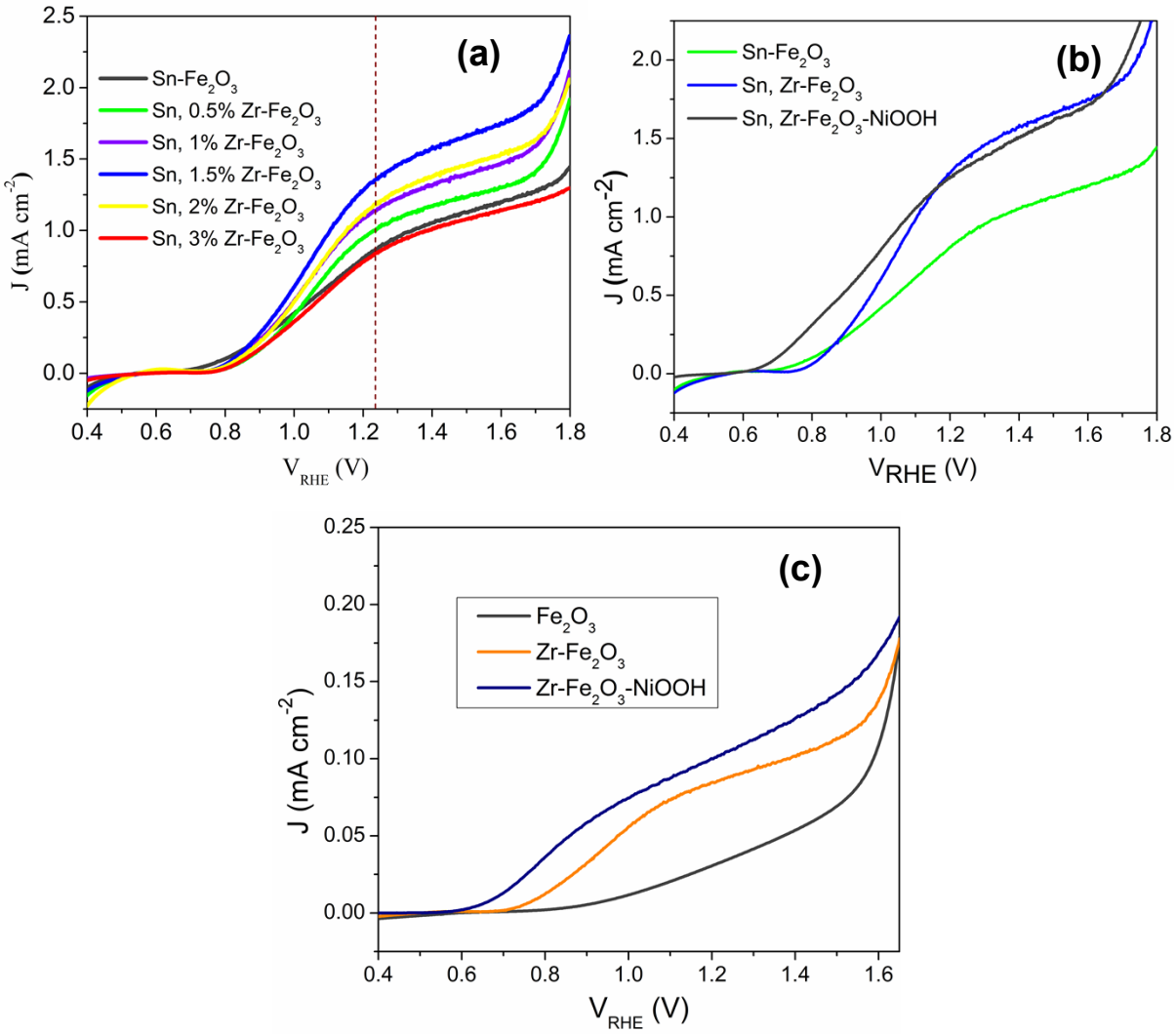

Figure S4. (a). J-V curves of codoped (Sn, Zr) Fe_2O_3 with different atomic percentage of Zr. (b) J-V curves of monodoped (Sn) Fe_2O_3, codoped (Sn, Zr) Fe_2O_3 and codoped (Sn, Zr) Fe_2O_3 modified with electrodeposited NiOOH. (c) J-V curves of pristine Fe_2O_3, Zr doped Fe_2O_3 and NiOOH coated Zr doped Fe_2O_3, Fe_2O_3 in all these three samples is annealed at 500 ^oC.

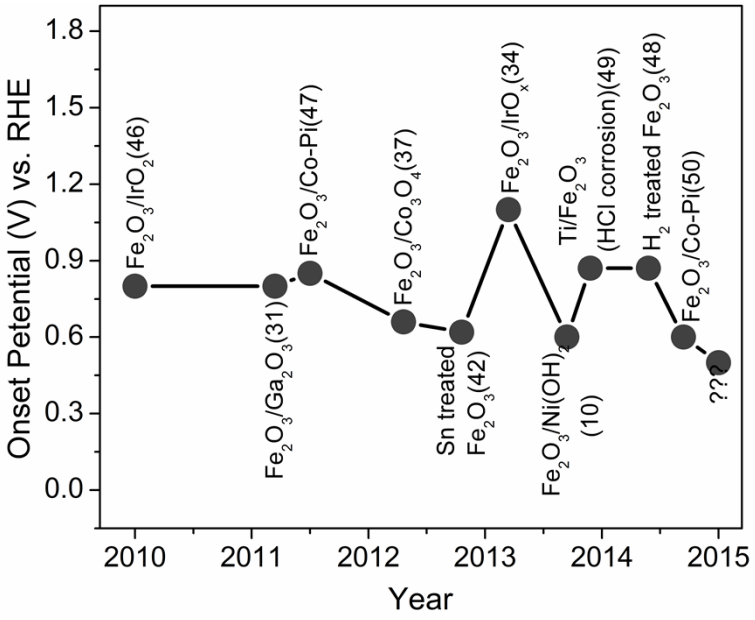

Figure S5. Recent historical achievements in the onset potential of surface modified hematite photoanodes presented in terms of photocurrent density generated under standard condition (1 sun).

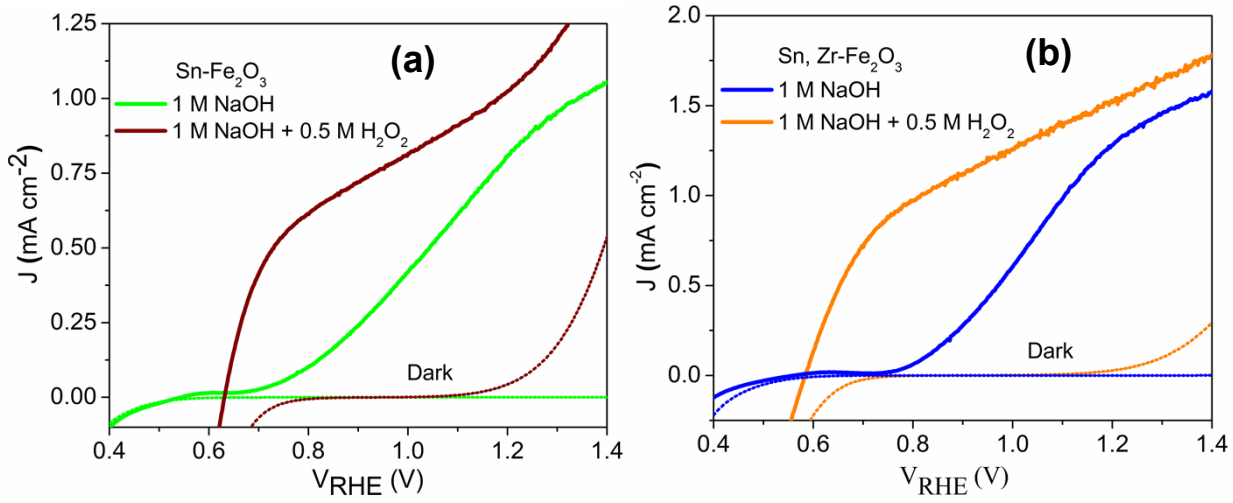

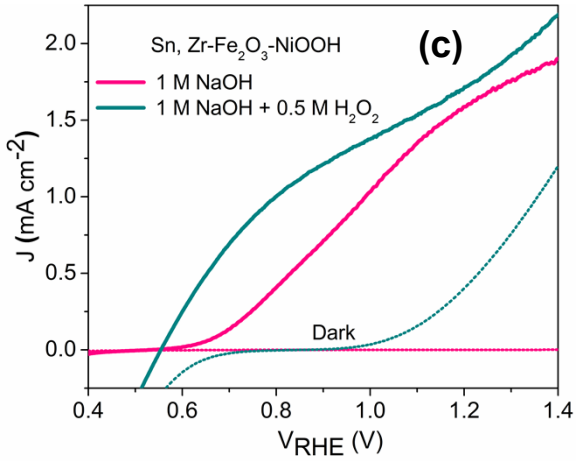

Figure S6. (a), (b) and (c) represent J-V curves in 1 M NaOH and 1 M NaOH + 0.5 M H_2O_2 electrolytes of monodoped (Sn) Fe_2O_3, codoped (Sn, Zr) Fe_2O_3 and NiOOH coated codoped (Sn, Zr) Fe_2O_3 electrodes respectively.

XPS characterization was conducted to verify the surface chemical composition of NiOOH modified codoped (Sn, Zr) Fe_2O_3 sample. The corresponding XPS spectrum of each element is shown below (Figure S7). From the XPS spectrum Fe, O, Sn, Zr and Ni signals can be clearly identified. There are three peaks in the O 1s fitted XPS spectra at 529.9, 531.8, and 533.4 eV. The peak at 529.9 eV is attributed to both the lattice oxygen of hematite and the [Ni-O] of NiOOH. The peak at 531.8 and 533.4 eV are identified as -OH surface groups and small amount of physically absorbed H_2O, respectively. The peak intensity in the Ni 2p XPS spectrum was low. This might be associated with the low loading amount of NiOOH. We further examined the amount of Sn using two different excitation energies, 800 and 1100 eV, which shows higher intensity at higher X-ray energy.

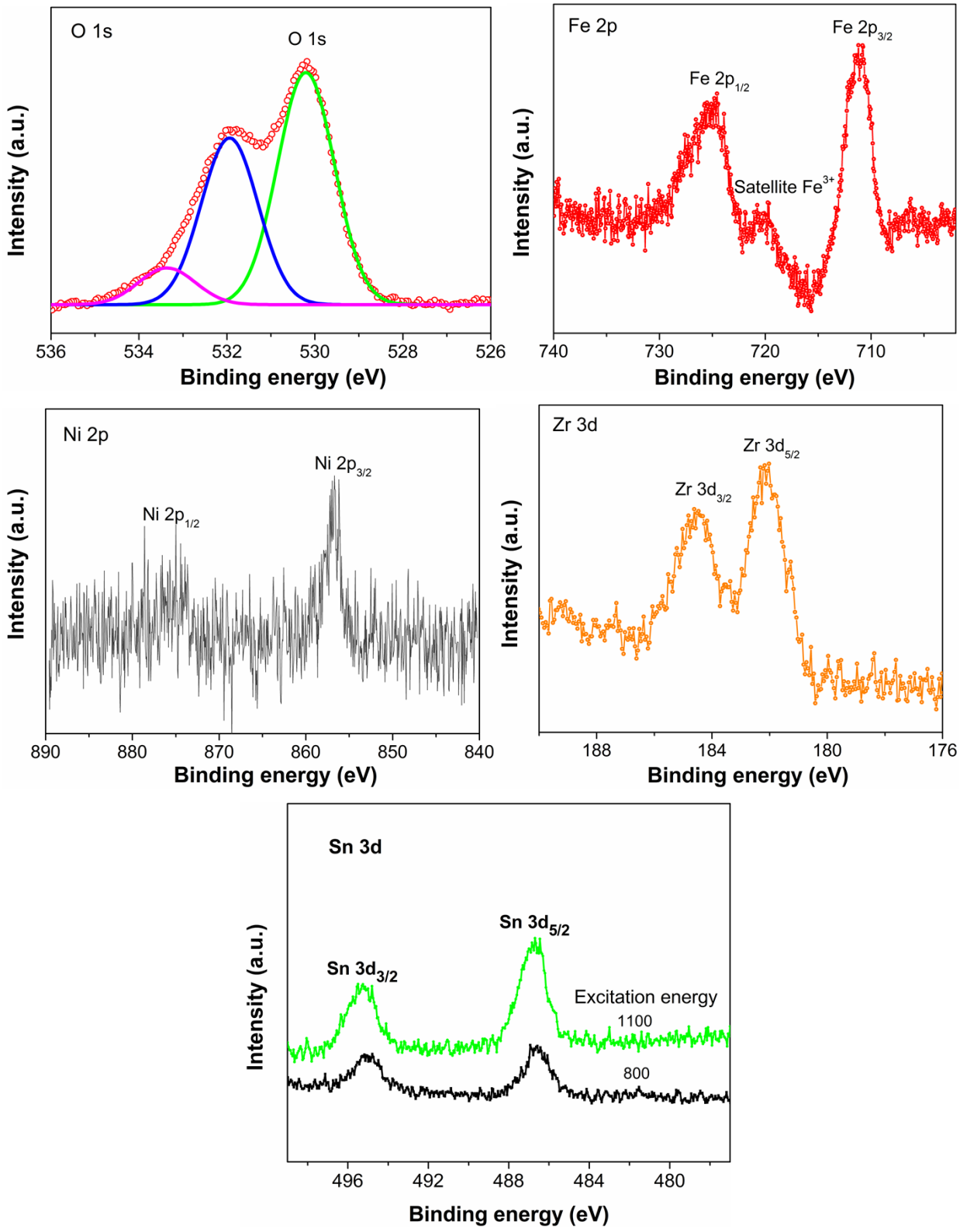

Figure S7. XPS spectra of NiOOH modified codoped (Sn, Zr) Fe_2O_3

Gas evolution test

Oxygen and hydrogen gases were collected using an air-tight monolithic reactor illustrated in Figure S8. The volume of gas collected was monitored by displacement of water. A magnetic stirrer was placed at the bottom of the reactor to remove dissolved oxygen from the electrolyte solution and to take out adsorbed gas from the surface of working electrode during photocatalytic water splitting. Before the photocatalytic water splitting reaction has begun, the reactor solution was purged with N_2 gas for 90 min. The codoped Fe_2O_3 sample modified with NiOOH was then illuminated with AM 1.5G (100 mW cm^{-2}) simulated solar light through the quartz glass window and 1.23 V potential was applied. The generated gases were collected by a water displacement gas trap, from which the volume of the actual gas generated can be determined. 0.2 mL of gas was extracted from the collected gas by a gas-tight micro syringe and analyzed by gas chromatography (GC) equipped with a Pulsed Discharge Helium Ionization Detector (PDHID). The amount of O_2 gas was noted every 30 minute time interval.

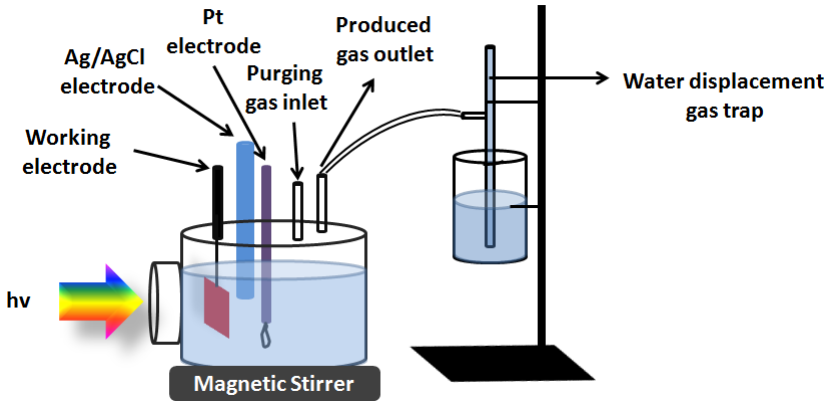

Figure S8. Schematic diagram of a typical reactor used for gas test.

In order to quantify the Faradaic efficiency, the volume of gas collected per area of electrode and time of gas evolution was recorded every 30 min and the number of moles of gas per area of electrode and time of gas evolution was calculated using the ideal gas law ($nO_2 = PV/RT$). Then the nO_2 is converted to photocurrent density (using photocurrent density = $4 \times nO_2 \times F$, where F is the Faraday constant which is 0.096487 C/μmol).

The Faradaic efficiency (FE) was then determined using the expression:

$$FE = \text{Actual photocurrent density/Theoretical photocurrent density}^{3}$$

Based on this calculation, the FE determined was found ranging from 90 to 96% during the whole measurements and the average Faradaic efficiency reached 93%. Thus, more than 90% of the photogenerated charges were consumed for water splitting and hydrogen/oxygen production in the current system.

Table S1. Faradaic efficiency calculated from PEC water oxidation results using NiOOH coated codoped Fe_2O_3 photoanode.

Time (h)	V of O_2 (L m^{-2} h^{-1})	nO_2 (μmol cm^{-2} s^{-1})	J calculated (mA cm^{-2})	J obtained from I-t (mA cm^{-2})	Faradaic Efficiency (%)
0	0	0	-	-	-
0.5	3.445	$3.92x10^{-3}$	1.51	1.66	90.96
1	3.578	$4.07x10^{-3}$	1.57	1.65	95.15
1.5	3.622	$4.12x10^{-3}$	1.59	1.65	96.36
2	3.511	$3.99x10^{-3}$	1.54	1.64	93.90
2.5	3.392	$3.86x10^{-3}$	1.49	1.64	90.85
3	3.357	$3.82x10^{-3}$	1.47	1.62	90.74
Average Faradaic efficiency (%)					**92.99**

References

1. P. Wang, D. Wang, J. Lin, X. Li, C. Peng, X. Gao, Q. Huang, J. Wang, H. Xu and C. Fan, *ACS Appl. Mater. Interfaces*, 2012, 4, 2295-2302.
2. Y.-H. C. a. K.-J. Tu, *Int. J. Photoenergy*, 2012, 2012, 1-6.
3. Y. Hou, F. Zuo, A. Dagg and P. Feng, *Angew. Chem. Int. Ed.*, 2013, 52, 1248-1252.